

THE ERROR DISTRIBUTION OF BATSE GRB LOCATIONS

MICHAEL S. BRIGGS¹, GEOFFREY N. PENDLETON¹, R. MARC KIPPEN², J. J. BRAINERD¹, KEVIN HURLEY³, VALERIE CONNAUGHTON⁴, CHARLES A. MEEGAN⁵To appear in *The Astrophysical Journal Supplement Series*

© 1999 by the American Astronomical Society.

1999 January 8

ABSTRACT

Empirical probability models for BATSE GRB location errors are developed via a Bayesian analysis of the separations between BATSE GRB locations and locations obtained with the InterPlanetary Network (IPN). Models are compared and their parameters estimated using 392 GRBs with single IPN annuli and 19 GRBs with intersecting IPN annuli. Most of the analysis is for the 4Br BATSE catalog; earlier catalogs are also analyzed. The simplest model that provides a good representation of the error distribution has 78% of the probability in a ‘core’ term with a systematic error of 1.85 degrees and the remainder in an extended tail with a systematic error of 5.1 degrees, implying a 68% confidence radius for bursts with negligible statistical uncertainties of 2.2 degrees. There is evidence for a more complicated model in which the error distribution depends on the BATSE datatype that was used to obtain the location. Bright bursts are typically located using the CONT datatype, and according to the more complicated model, the 68% confidence radius for CONT-located bursts with negligible statistical uncertainties is 2.0 degrees.

Subject headings: gamma rays: bursts, observations — methods: statistical

1. INTRODUCTION

An improved model for the distribution of errors for gamma-ray burst (GRB) locations obtained with the Burst and Transient Source Experiment (BATSE) is presented. The error model should aid in using the BATSE locations in projects such as searching for counterparts and searching for evidence of repetition and clustering, including gravitational lensing. Most of the analysis applies to the 4Br catalog (Paciesas et al. 1998), which has some revised locations compared to earlier catalogs, including the initial 4B catalog (Paciesas et al. 1997), which was released electronically and on CDROM. Summary results are presented for earlier catalogs.

The BATSE instrument consists of eight modules located on the corners of the Compton Gamma-Ray

Observatory (CGRO). Each module contains a Large Area Detector (LAD), consisting of a 1.27 cm thick by 50.8 cm diameter NaI crystal viewed by three photomultiplier tubes. Each LAD has an approximately cosine response. GRB locations are determined with the program LOCBURST by modeling the responses of either four or six detectors as a function of assumed source location, intensity and spectrum (Pendleton et al. 1998). The detector response model is based upon Monte Carlo photon propagation, laboratory measurements and space observations. It includes scattering from nearby spacecraft structures and from the earth’s atmosphere (Pendleton et al. 1995, 1998).

The error models presented in this paper are obtained empirically by statistical comparison of

¹Department of Physics, University of Alabama in Huntsville, Huntsville, AL 35899

²Center for Space Plasma, Aeronomic and Astrophysics Research, University of Alabama in Huntsville, Huntsville, AL 35899

³Space Sciences Laboratory, University of California, Berkeley, CA 94720-7450

⁴NRC & NASA/Marshall Space Flight Center, Huntsville, AL 35812

⁵NASA/Marshall Space Flight Center, Huntsville, AL 35812

BATSE locations with locations obtained by other techniques. The ideal reference dataset would have many locations to enable a good statistical comparison and would consist of locations with errors significantly smaller than the BATSE errors so that all discrepancies could be attributed to BATSE. If such a dataset existed, there would probably be little interest in the BATSE locations. The reference set we use is the locations of the InterPlanetary Network (IPN) Supplements to the BATSE 4Br catalog (Hurley et al. 1998a,b; Laros et al. 1997,1998; Hurley 1998). Although this dataset is large, most of the IPN locations are highly accurate only in one dimension.

2. ANALYSIS APPROACH

2.1. *The Problem*

The goal is an improved model of the error distribution of BATSE GRB locations. The error model is a probability density function p defined on the sphere. A probability density function can have any nonnegative value; integrating p with respect to solid angle element $d\Omega$ over any solid angle region Ω yields the probability P (between 0 and 1) that the true location is in the region Ω .

A portion of the errors originates from the Poisson fluctuations of the detected counts. These fluctuations are propagated into an estimated statistical uncertainty σ_{stat} by the program LOCBURST. The locations are found by LOCBURST by χ^2 -minimization, and σ_{stat} is calculated as the radius of the spherical small circle with the same area as the 68% confidence ellipse obtained from the Hessian matrix of derivatives of χ^2 (Pendleton et al. 1998). In this paper we assume that the total error distribution is azimuthally symmetric. The value of σ_{stat} for each GRB is listed in the 4Br catalog (Paciesas et al. 1998), or, for bursts with unchanged locations, in the 3B catalog (Meegan et al. 1996). We attribute the difference between the total error σ_{tot} and the statistical uncertainty σ_{stat} to a systematic error σ_{sys} . Possible sources of systematic errors include: inaccuracies in the assignment of energies to channel boundaries, inaccuracies in the deadtime correction of high count rates, the approximations of the statistical and total error boxes as circles, inaccuracies in the detector response model as a function of photon energy or direction, including inaccuracies in the model of scattering from the spacecraft and the earth's atmosphere, deviations of the actual GRB spectra from the power law assumed in most cases, and inaccuracies in background subtraction.

The first published BATSE catalog, the 1B catalog

(Fishman et al. 1994), had 260 GRBs. The error estimate was based on eleven events with small error boxes from IPN data. A root-mean-square difference between the actual BATSE-IPN separations and the BATSE statistical uncertainties estimated a systematic error of $\sigma_{\text{sys}} = 4^\circ$ (Fishman et al. 1994). The 3B catalog (Meegan et al. 1996) introduced an improved location algorithm. The analysis of the 3B location errors expanded the reference dataset to include 38 locations obtained with CGRO/COMPTEL or WATCH in addition to 12 IPN locations. The systematic error σ_{sys} was estimated to be 1.6° from the root-mean-square difference between the actual separations to these 50 reference locations and the BATSE statistical uncertainties. The total errors of the COMPTEL or WATCH locations are not much smaller than the BATSE errors; in this situation a very good understanding of the errors of the reference locations is required, otherwise the portion of the location discrepancies due to BATSE may be miscalculated. An overestimation of the COMPTEL or WATCH location errors may have caused the BATSE systematic error to be somewhat underestimated. In addition, we show that the BATSE error distribution is not well characterized by a single-valued systematic error so that various techniques of estimating a single systematic error yield different values (see, e.g., Pendleton et al. 1998).

We term the simple error model specified in the 3B paper (Meegan et al. 1996), that the total error σ_{tot} is formed by adding the statistical uncertainty σ_{stat} and a systematic error σ_{sys} of 1.6° in quadrature, the “minimal” model.

A rough rule of thumb learned in this analysis is that with N reference locations, models with up to $\sim N/50$ parameters may be fit. Exceeding this empirical limit typically results in models difficult or impossible to fit, and, if a fit is obtained, nonsense parameter values. There are only about 20 ‘point’ locations available from IPN data, but by using a more sophisticated analysis method (Graziani and Lamb 1996), the several hundred single annuli in the IPN Supplements may be used to constrain the BATSE location error distribution. Formerly representations of the systematic error were limited to using a single parameter; considerably more complicated error models can now be tested.

2.2. *Reference Data*

The IPN location technique compares the arrival times of the GRB wavefront at widely separated instruments, thereby determining the angles the plane

wave makes with the vectors connecting each pair of instruments (Hurley et al. 1998a). With only one pair of spacecraft, one angle is determined, and the error region is an annulus. This is the typical case during the time period of the 4B catalog. Ideally, three or more spacecraft have separations of interplanetary scale, multiple annuli are found, and their intersections give a small error box. The IPN Supplements to the 4Br catalog contains 458 annuli for 412 GRBs. Of these 412 GRBs, 366 were observed by only one deep-space instrument, *Ulysses* (Hurley et al. 1998a,b). The remaining 46 GRBs were observed by *Ulysses* and another deep-space instrument such as Pioneer Venus Orbiter or Mars Observer (Laros et al. 1997,1998).

Measurements of the actual separations γ are available for the few cases with small error boxes from intersecting IPN annuli. For the cases for which only single annuli are available, the BATSE-IPN separations are characterized by the distances of closest approach ρ of the annuli to the BATSE locations (Fig. 1).

Our analysis approach assumes that the reference locations are effectively points or lines compared to the BATSE locations, an assumption which is fulfilled by eliminating all annuli with 3σ widths exceeding 1.6° and eliminating 3σ error boxes with any corner-to-corner dimension exceeding 1.6° . Because there are few IPN annuli with large widths, decreasing or increasing the 1.6° requirement by a factor of two leads to only small changes in the number of annuli included in the comparison sample and negligible changes in the results. We convert the annuli to circles on the sphere, or their intersections to points, by using the circle in the middle of each annulus. Each pair of annuli has two intersections—we assume that the intersection closest to the BATSE location is the true location. Many of the intersecting annuli create long error boxes which are rejected by the requirement that no dimension exceed 1.6° , in which case we keep only the narrowest annulus. Such error boxes are common during the time period of the 4Br catalog because frequently several of the spacecraft of the Third Interplanetary Network have been close in space. The vectors connecting each pair of spacecraft define the centers of the annuli, and with some spacecraft in similar directions, these vectors are typically close to parallel. This leads to ‘grazing’ intersections of the annuli and long error boxes. (An additional consequence of grazing intersections is that a small error in one annulus will move the intersection a comparatively large distance). After

removing the wide annuli and large error boxes, 430 annuli for 411 GRBs remain. For GRBs with intersecting annuli meeting our criteria and therefore with a measurement of γ , we do not use the two measurements of ρ that could be obtained from the individual annuli, thereby ensuring the independence of all the γ and ρ measurements. These criteria yield a reference dataset with 19 measurements of γ and 392 measurements of ρ .

The 411 GRBs with IPN locations meeting our criteria represent 25% of the 1637 GRBs of the 4Br catalog. The relative sensitivities of BATSE and the deep-space instruments of the Third Interplanetary Network are largely determined by their effective areas and by their backgrounds. Each BATSE LAD has an effective area of 2025 cm^2 , compared to, for example, a projected area of 20 cm^2 for *Ulysses*. The differences in sensitivities are not as great as the comparisons of areas would indicate because the deep-space instruments have lower and more stable backgrounds. Fig. 2 compares the properties of the bursts of the 4Br catalog with the bursts of the IPN Supplements to the 4Br catalog. The IPN Supplements sample almost the entire range of peak fluxes on the 64 ms timescale of the 4Br catalog, albeit with emphasis on the bright bursts. In terms of fluence, the IPN Supplements have a strong bias towards bright bursts, with only rare events below $10^{-6} \text{ erg cm}^{-2}$ having IPN annuli. There is a close correlation between burst fluence and BATSE σ_{stat} , so a similar effect is seen in the distributions of σ_{stat} .

2.3. Bayesian Model Comparison

If many ‘point’ reference locations were available, a histogram of the observed separations γ between the BATSE locations and the reference locations would provide a good representation of the probability distribution of BATSE errors. Because most of the reference locations from the IPN Supplements are single annuli, insufficient information exists for such a simple approach. Instead the error function $p(\gamma)$ is determined by comparing models for $p(\gamma)$ and optimizing their parameters using the entire dataset of γ and ρ measurements.

A Bayesian analysis very similar to that of Graziani and Lamb (1996) is used to identify the best error model. The Bayesian approach identifies the likelihood function as the correct ‘merit’ function (Sivia 1996). The likelihood function L is simply the product of the probability density functions p evaluated at each observed value of γ for bursts i with intersecting annuli and at each observed value of ρ

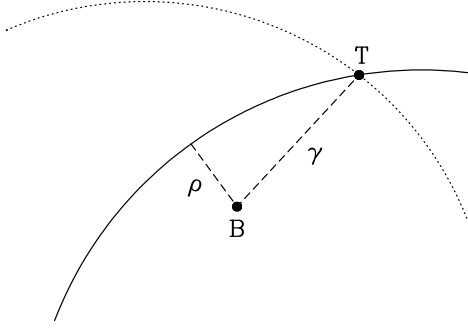


FIG. 1.— If two thin IPN annuli are available (solid and dotted arcs), then we assume that their intersection gives the true location \hat{T} . In this case the angle γ between the true location \hat{T} and the BATSE location \hat{B} is known. If only one IPN annulus is available (solid arc), the position of the true location on the annulus is unknown, and the separation between the annulus and BATSE location \hat{B} is characterized by the angle of closest approach ρ .

for bursts j with single annuli:

$$L = \prod_i p_\gamma(\gamma_i) \prod_j p_\rho(\rho_j). \quad (1)$$

The probability density function p_ρ used for the single annuli cases is analytically derived from p_γ (see Appendix). The likelihood function identified by the Bayesian method specifies how measurements of differing nature (intersecting vs. single annuli) are to be combined in the analysis. While eq. 1 shows the likelihood L as a function of the observations, L is also, through the functions p_γ and p_ρ , a function of the error model and its parameters. For a particular error model, the best-fit parameters are obtained by maximizing the likelihood.

An additional consideration arises in comparing models: a model with more parameters than another must be penalized because it has greater ability to match the data whether or not it is correct. The Bayesian approach specifies how this must be done: each model is penalized by an Occam's factor F . Assuming that prior to examining the data one expects parameter λ_k to be in the range λ_k^{\min} to λ_k^{\max} and that the likelihood function is approximately Gaussian, these factors are, per parameter λ_k (Sivia 1996),

$$F_k = \frac{\sigma_{\lambda_k} \sqrt{2\pi}}{\lambda_k^{\max} - \lambda_k^{\min}}, \quad (2)$$

where σ_{λ_k} is the uncertainty on λ_k obtained from the fit. The overall Occam's factor F is the product of the F_k and penalizes a model for obtaining a better fit by using adjustable parameters, with a greater penalty (smaller F) when the parameters have larger possible prior ranges.

The final consideration is that one might have prior preferences for particular models from earlier analyses or judgments. These preferences can be represented as prior probabilities for each model $P_{\text{prior}}(M)$.

Combining these considerations, the Odds ratio $O_{B/A}$ specifies the factor by which one should prefer model B over model A:

$$O_{B/A} = \frac{P(B)}{P(A)} = \frac{P_{\text{prior}}(B) \times L(B) \times F(B)}{P_{\text{prior}}(A) \times L(A) \times F(A)}. \quad (3)$$

To avoid suspicions that our beliefs have created the results, we equate all prior probabilities so that the first factor in eq. 3 cancels. Many of the models have common parameters so that some of the Occam's factors F_k also cancel. For most of the model comparisons the likelihood ratios are so large that no reasonable priors nor Occam's factors F could alter which model is identified as best.

Further discussion of Bayesian methodology, model fitting and comparison are given by Sivia (1996) and Loredó (1990).

Instead of listing the odds ratios $O_{B/A}$ for every combination of models A and B, we list what we call odds factors O_M for each model M. The odds factors O_M are proportional to $P(M)$ by a factor which is the same for each model, therefore the odds ratios $O_{B/A}$ can be found by forming the ratio of the factors O_B and O_A , or by differencing their logarithms (Tables 2 and 5). The likelihoods and parameter uncertainties are also listed (Tables 2 and 3) so that others can calculate odds ratios based upon their priors.

While the quantitative analysis is done with unbinned data using likelihood, we prefer to depict the data and models with histograms (Fig. 3–5, 7 & 9). In order to present the results in a consistent manner, the data and models are binned using the total errors of the minimal model, $\sigma_{\text{tot}}^0 = (\sigma_{\text{stat}}^2 + 1.6^\circ)^{1/2}$.

2.4. Probability Models

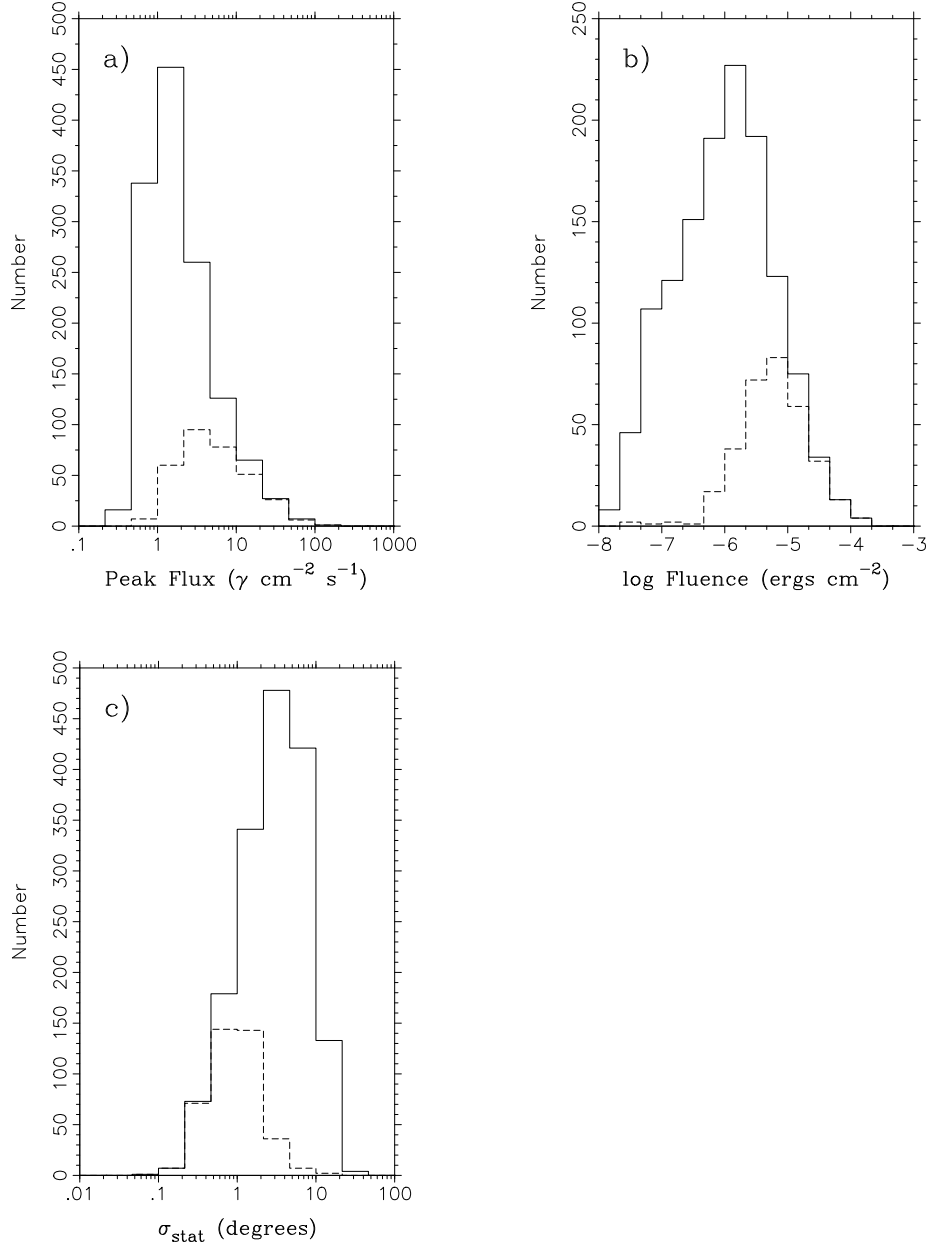


FIG. 2.— Comparison of bursts for which BATSE triggered (solid histograms) with the subset in the IPN Supplements (dashed histograms). a) The distributions of peak flux as observed by BATSE between 50 and 300 keV on the 64 ms timescale. There are 1292 bursts in the 4Br catalog with flux/fluence values (solid histogram), of which 324 are also in the IPN Supplements (dashed histogram). b) The distributions of fluence as observed by BATSE between 50 and 300 keV of the same groups of 1292 and 324 bursts. c) The distributions of BATSE σ_{stat} for all 1637 GRBs of the 4Br catalog (solid histogram) and for the subset of 411 events with IPN data meeting our criteria (dashed histogram).

We define the total error as the quadratic sum of the statistical uncertainty σ_{stat} (as listed in the 4Br catalog) and a systematic error:

$$\sigma_{\text{tot}} = (\sigma_{\text{stat}}^2 + \sigma_{\text{sys}}^2)^{1/2}. \quad (4)$$

Our error models are based on the Fisher probability density function p_F , which has been called the Gaussian distribution on the sphere:

$$p_F(\gamma) d\Omega = \frac{\kappa}{2\pi(e^\kappa - e^{-\kappa})} e^{\kappa \cos \gamma} d\Omega, \quad (5)$$

where γ is the angle between the measured and true location (Fisher et al. 1987). The first convenience of this distribution is that it is normalized on the sphere and that the ‘volume’ element is clearly solid angle $d\Omega$. The distribution also has convenient analytic properties; in the small angle approximation it reduces to the Gaussian distribution. An algorithm to simulate random locations from a Fisher distribution is given by Fisher et al. (1987).

The probability P of the true location lying in a region of solid angle Ω is found by integrating the probability density function p :

$$P = \frac{\kappa}{2\pi(e^\kappa - e^{-\kappa})} \int_{\Omega} d\Omega e^{\kappa \cos \gamma}. \quad (6)$$

Specializing to the probability of the true location being in the ring $\gamma_1 \leq \gamma \leq \gamma_2$, eq. 6 becomes

$$P = \frac{\kappa}{e^\kappa - e^{-\kappa}} \int_{\gamma_1}^{\gamma_2} d\gamma \sin \gamma e^{\kappa \cos \gamma}. \quad (7)$$

The parameter κ is termed the concentration parameter. BATSE GRB location errors have traditionally been specified in terms of σ , which has been defined by the BATSE team as the radius of the circle with the same area as the 68% confidence ellipse. Assuming the error box to be circular, and setting $P = 0.68$, $\gamma_1 = 0$ and $\gamma_2 = \sigma_{\text{tot}}$ in eq. 7, one obtains, for σ_{tot} in *radians* and for σ_{tot} small ($\lesssim 20^\circ$):

$$\kappa = \frac{1}{(0.66\sigma_{\text{tot}})^2}. \quad (8)$$

Models more complicated than a Fisher distribution are tested. The first method of building more complicated models is to make σ_{sys} a function of either intrinsic burst properties or of instrumental factors which might influence the quality of locations. The second way in which more complicated models

are formed is to sum two Fisher distributions with different values of σ_{sys} :

$$p = f_1 p_F^1 + (1 - f_1) p_F^2. \quad (9)$$

In this case, for each burst, the values of the two total location errors $\sigma_{\text{tot},i}$ are calculated from the statistical uncertainties σ_{stat} listed in the catalog and the model values $\sigma_{\text{sys},i}$ (for $i = 1, 2$):

$$\sigma_{\text{tot},i} = (\sigma_{\text{stat}}^2 + \sigma_{\text{sys},i}^2)^{1/2}. \quad (10)$$

For the single annulus cases, the probability density function $p(\rho)$ is analytically derived from the probability density function $p(\gamma)$ (see Appendix). Since $\rho \leq \gamma$ (see Fig. 1), $P(\rho < X) > P(\gamma < X)$. Table 1 gives some cumulative probabilities P for both $p_F(\gamma)$ and the corresponding $p(\rho)$.

3. RESULTS

3.1. 4Br Catalog

The systematic error of 1.6° used in the minimal model was determined using 50 comparison locations, some of which had errors not much smaller than the BATSE errors (Meegan et al. 1996). Fig. 3 compares the 4Br data to the minimal model—with the large and accurate IPN reference dataset, the minimal model is clearly seen to be a poor fit to the data. Model 1 generalizes the minimal model by optimizing the value of the systematic error, obtaining 2.8° . While a major improvement over the minimal model, this model fits the data poorly (Fig. 4) and has a much smaller odds factor than some other models (Table 2).

The value of 1.6° published in the 3B catalog (Meegan et al. 1996) was determined by a root-mean-square comparison of the observed separations with the combination of the BATSE statistical uncertainties and the known errors of the reference locations. The 3B catalog warned that some locations might be substantially worse than average and that the error distribution might have a non-Gaussian tail.

Model 2 implements the idea of a Gaussian-like distribution with an extended tail by summing two Fisher distributions having differing systematic errors (eqs. 9 and 10). This model provides an excellent fit to the data (Fig. 5 and Table 2). The evidence favors Model 2 over the minimal model by an odds ratio of 10^{56} and over Model 1 by 5×10^7 (Table 2). The best-fit parameters are given in Table 3.

Model 2 is best thought of as a ‘core-plus-tail’ representation of the error distribution rather than as a two-component model. The model does not specify

TABLE 1
 CUMULATIVE VALUES FOR THE DISTRIBUTIONS OF γ AND ρ ASSUMING THE FISHER DISTRIBUTION

Angle X	$P_{\text{F}}(\gamma \leq X)$	$P(\rho \leq X)$
1σ	0.6826	0.8703
2σ	0.9898	0.9976
3σ	>0.9999	>0.9999

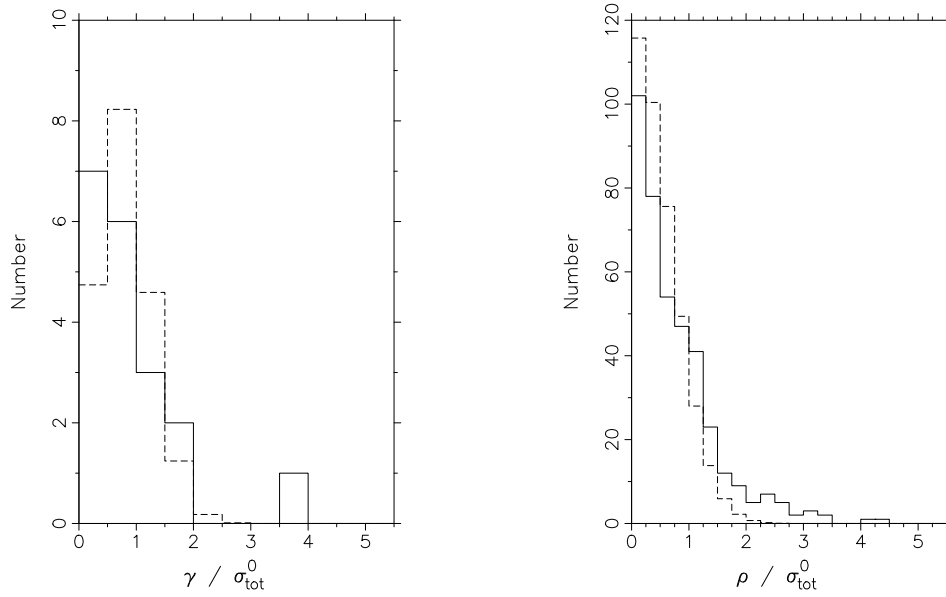


FIG. 3.— Histograms of the data (solid) and Model 0 (dashed) for the separations γ between BATSE locations and intersecting IPN annuli and the closest separations ρ between BATSE locations and single IPN annuli. The data and model are binned in terms of $\sigma_{\text{tot}}^0 = (\sigma_{\text{stat}}^2 + 1.6^\circ)^{1/2}$. The data and Model 0 are clearly in poor agreement.

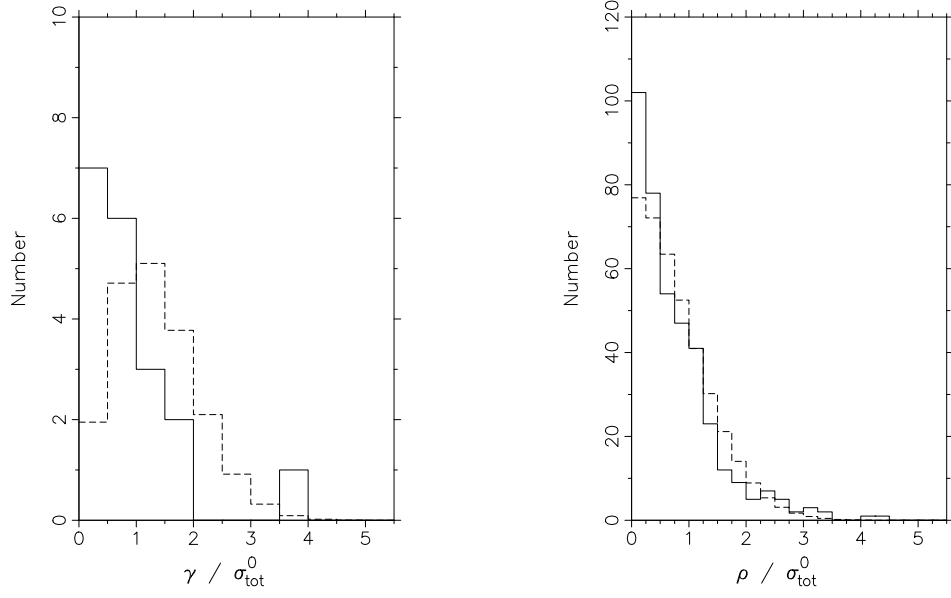


FIG. 4.— Histograms of the data (solid) and Model 1 (dashed). Model 1 predicts too few events at both small ($\rho/\sigma_{\text{tot}}^0 \lesssim 0.25$) and large ($\rho/\sigma_{\text{tot}}^0 \gtrsim 3$) separations.

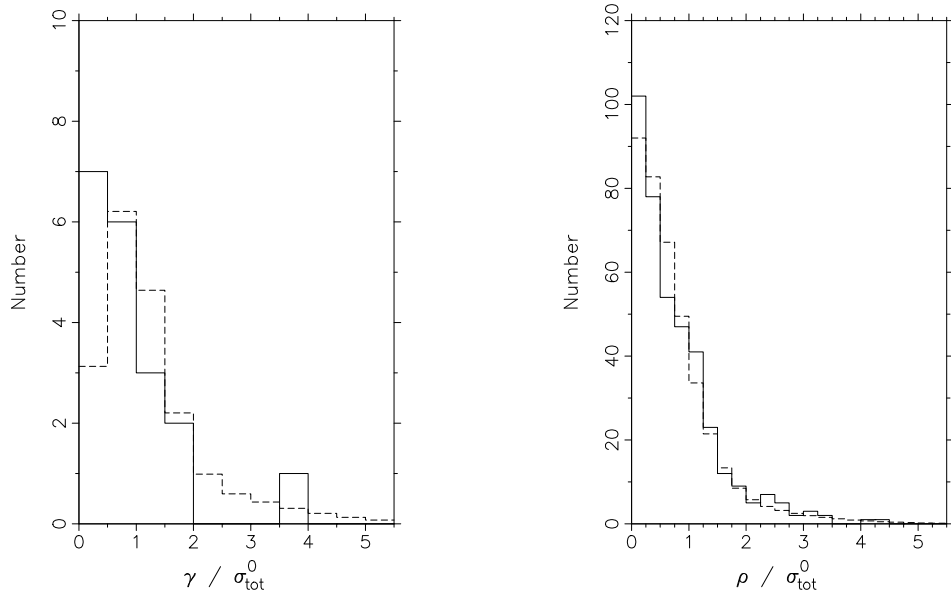


FIG. 5.— Histograms of the data (solid) and Model 2 (dashed). The agreement between the data and Model 2 is excellent.

TABLE 2
MODEL COMPARISON RESULTS FOR 4BR CATALOG

Model	Description	Number of Parameters	\log_{10} likelihood	\log_{10} Odds Factor
0	Minimal: Systematic Error Assumed to be 1.6°	0	161.5	161.5
1	Single Systematic Error applied to all locations	1	211.5	210.2
2	Core-plus-Tail Systematic Errors	3	220.8	217.9
4	Systematic Error a power law function of statistical uncertainty: $\sigma_{\text{sys}} = A(\sigma_{\text{stat}}/1^\circ)^\alpha$	2	212.6	210.4
10	Core-plus-tail Systematic Errors depending on datatype	6	223.7	219.4
12	Core-plus-tail for CONT, one systematic error for other datatypes	4	222.9	219.0
33	Core-plus-tail, only core systematic error depends on datatype	4	223.6	219.9

TABLE 3
BEST-FIT ERROR MODEL PARAMETER VALUES FOR THE 4BR CATALOG

Model	Symbol	Parameters Description	Value [†]
1	σ_{sys}	Systematic Error	2.80 ± 0.12
2	σ_{sys}^1	Core systematic error	$1.85^\circ \pm 0.16^\circ$
	f_1	Fraction in Core Term	0.78 ± 0.08
	σ_{sys}^2	Tail systematic error	$5.1^\circ \begin{smallmatrix} +0.8 \\ -0.6 \end{smallmatrix}$
4	A	Amplitude (error for $\sigma_{\text{stat}} = 1^\circ$)	2.93 ± 0.13
	α	Power law index	0.14 ± 0.06
10	σ_{CONT}^1	Core systematic error for CONT	$1.68^\circ \pm 0.16^\circ$
	f_{CONT}^1	Fraction in Core Term for CONT	$0.82 \begin{smallmatrix} +0.05 \\ -0.08 \end{smallmatrix}$
	σ_{CONT}^2	Tail systematic error for CONT	$5.3^\circ \begin{smallmatrix} +1.0 \\ -0.8 \end{smallmatrix}$
	σ_{other}^1	Core systematic error for non-CONT	$2.6^\circ \pm 0.5^\circ$
	f_{other}^1	Fraction in Core Term for non-CONT	$0.73 \begin{smallmatrix} +0.19 \\ -0.35 \end{smallmatrix}$
	σ_{other}^2	Tail systematic error for non-CONT	$5.2^\circ \begin{smallmatrix} +2.1 \\ -1.2 \end{smallmatrix}$
12	σ_{CONT}^1	Core systematic error for CONT	$1.67^\circ \pm 0.15^\circ$
	f_{CONT}^1	Fraction in Core Term for CONT	$0.82 \begin{smallmatrix} +0.05 \\ -0.08 \end{smallmatrix}$
	σ_{CONT}^2	Tail systematic error for CONT	$5.3^\circ \begin{smallmatrix} +1.0 \\ -0.8 \end{smallmatrix}$
	σ_{other}^1	Systematic error for non-CONT	$3.44^\circ \pm 0.26^\circ$
33	σ_{CONT}^1	Core systematic error for CONT	$1.67^\circ \pm 0.15^\circ$
	σ_{other}^1	Core systematic error for other	$2.74^\circ \pm 0.34^\circ$
	f_{all}^1	Fraction in Core, all datatypes	$0.82 \begin{smallmatrix} +0.05 \\ -0.07 \end{smallmatrix}$
	σ_{all}^2	Tail systematic error for all datatypes	$5.4^\circ \pm 0.8^\circ$

[†]The uncertainties on the parameter values are for single parameters of interest (i.e., they were obtained from the change in likelihood equivalent to the usual $\chi^2 + 1$ prescription). In some cases the uncertainties between the parameters are highly correlated. However, further specification of the errors on the errors of the locations would be excessive.

that some bursts belong to a core component (small σ_{sys}) and others to a tail component (large σ_{sys}); instead all bursts have a tail to their location error distribution. Model 2 uses no burst property other than σ_{stat} to determine the location error distribution of each burst.

To depict the distribution of separations γ between the BATSE location and the true location given by Model 2, we perform part of the solid angle integration over the sphere of the probability density function p_2 of Model 2:

$$1 = \int_0^\pi d\gamma \int_0^{2\pi} d\psi \sin \psi p_2(\gamma) \quad (11)$$

$$= \int_0^\pi d\gamma \frac{dP_2}{d\gamma}(\gamma). \quad (12)$$

The function $dP_2/d\gamma$ is depicted in Fig. 6 for a burst with a negligible value for σ_{stat} . The ‘core’ and ‘tail’ terms are shown separately along with the total model. While 22% of the probability is in the tail term, much of the area of the tail term is near $\gamma = 0$ so that only 7% of the locations are past $\gamma = 5^\circ$.

We have endeavored to find correlations that would allow us to assign σ_{sys} values based upon burst or location properties, either by fitting models with σ_{sys} a function of the property, or by dividing the locations into categories by the property and comparing the values of model parameters. Among the properties for which no significant dependence was found are: the fluence of the burst, the value of σ_{stat} , the χ^2 -value obtained by LOCBURST, the angle to the center of the earth (which affects the importance of atmospheric scattering), the spectral index of the burst, and whether the event was a *Ulysses* trigger or was obtained from *Ulysses* continuous data. In a test for a dependence of location quality on spacecraft scattering, we made three extensions each of Models 1 and 2, adding a parameter dependence on the spacecraft hemisphere (+/-X, +/-Y, or +/-Z) in which the burst was located. The coordinate system is defined so that COMPTEL and EGRET view in the +Z direction and OSSE scans in the XZ plane (Gehrels, Chipman & Kniffen 1993). The motivation is that the spacecraft is not symmetrical in Y and Z, and inadequacies in the modeling of the scattering from the spacecraft might cause location quality to depend on position in spacecraft coordinates. There were modest odds ratios improvements for two of the extensions of Model 1 (not approaching the odds ratio of Model 2), but none for the extensions of Model 2. We conclude that the bilateral asymmetries of the

spacecraft do not create bilateral asymmetries in location quality.

The only property that we have identified as significant is the type of the data used to obtain the location. In addition to four continuously transmitted ‘background’ datatypes, the BATSE instrument packages data from triggered events into eight burst datatypes. Any of the background or burst datatypes which include data separately from each of the LADs can be used to derive a location. The default datatype for locating bursts is CONT, which provides continuous coverage regardless of trigger status in 16 energy channels with 2 s time resolution. The CONT datatype was used for 58% of the locations in the 4Br catalog. If the event is shorter than 2 s, so that using CONT data would unnecessarily add statistical fluctuations, or if CONT data are unavailable due to a telemetry gap, discriminator data (DISCLA, DISCLB, PREB or TTE) with four energy channels are used. If normal telemetry is available, 1 s resolution DISCLA would typically be used. A duplicate of DISCLA data, DISCLB, is included in the burst data to obtain more reliable telemetry. Together DISCLA and DISCLB data were used for 23% of the locations. The instrument triggers at the end of the interval in which a significant rate increase is registered. If the burst has essentially ended by the trigger time, then one of the high-time resolution pre-burst datatypes is used, either PREB or TTE. This was the case for 12% of the locations. Finally, if no regular data are available due to missing telemetry, the maximum rates recorded by the instrument during the burst readout are used (MAXBC or MAXC1). This was necessary for 8% of the 4B locations. (The percentages sum to 101% due to rounding.)

Models 10, 12 (§3.2) and 33 incorporate correlations between location accuracy and datatype. Model 10 is very similar to Model 2, with the difference that the model parameter values depend on the datatype. One set of model parameters like those of Model 2 are used for locations obtained using CONT data, σ_{CONT}^1 , f_{CONT}^1 , and σ_{CONT}^2 , while another set, σ_{other}^1 , f_{other}^1 , and σ_{other}^2 , is used for all other locations. Model 10 has a likelihood $\times 800$ larger than that of Model 2 (Table 2). Considering the three additional parameters, the odds ratio favors Model 10 by a factor of 30.

Two pairs of parameters of Model 10, f_{CONT}^1 & f_{other}^1 and σ_{CONT}^2 & σ_{other}^2 , have values which are consistent (see Table 3), i.e., the data do not demonstrate that these parameters have different values. This suggests a model with fewer parameters: Model 33 has

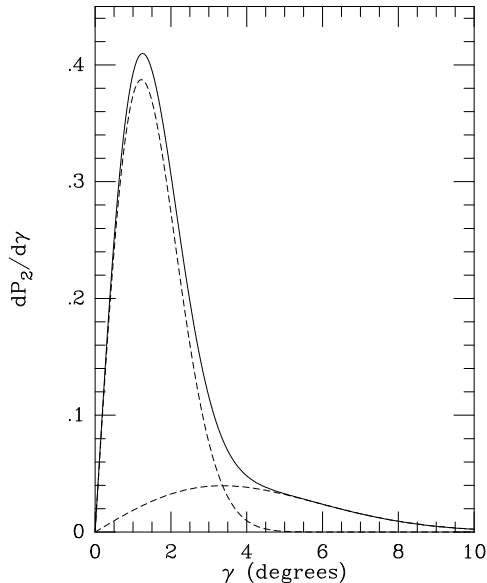


FIG. 6.— The function $dP_2/d\gamma$ (eqs. 11 and 12) is the error distribution versus separation γ according to Model 2. It is shown for a gamma-ray burst with a negligible value for σ_{stat} . The function as depicted includes the solid angle factor $2\pi \sin \psi$. If this factor were not included, the function would be very large near $\gamma = 0$, yet the probability of very small γ is low because of the solid angle factor. The integral from $\gamma = 0$ to 180° of the function shown is one. The solid curve shows Model 2 (as specified in Table 3), while the dashed curves show the two terms, ‘core’ and ‘tail’, separately.

distinct parameter values for the core systematic errors of CONT-derived locations and locations obtained with other data types, but only a single parameter f_{all}^1 representing the probability of the core term, and only a single tail systematic error σ_{all}^2 . The likelihood ratios of Models 10 and 33 are virtually identical; because of the fewer parameters of Model 33 its odds ratio is $\times 3$ better (Table 2). This improvement may mean that the ‘tail’ is caused by factors independent of datatype, or simply that there is insufficient data to discern differences in the tail as a function of datatype. The odds ratio improvement is marginal and the models make very similar predictions, so an explanation is not required. Model 33 is favored over Model 2 by an odds ratio of 100. Qualitatively, this might be termed as persuasive but not compelling evidence for Model 33 over Model 2. The data and Model 33 are compared in Fig. 7.

Locations obtained with datatypes other than CONT, i.e., using either PREB, TTE, DISCLA, DISCLB, or MAXBC datatypes, are consistent with being of equal quality. However, of the 411 bursts with reference IPN locations, only 110 were located with datatypes other than CONT, so the comparisons are probably insensitive.

The Bayesian approach relies upon model comparisons rather than goodness-of-fit tests—generally one does not know whether a particular best-fit value of the likelihood is reasonable. As a final test of the quality of the models, we (not being doctrinaire Bayesians) perform goodness-of-fit tests via simula-

tions. Assuming a specific model to be true, we simulate datasets of BATSE locations using the best-fit parameters of the model. We use the actual IPN annuli, pick locations on single annuli and on the intersection of each pair to be the ‘true’ locations, and then create simulated BATSE locations using the assumed error model. The separations between the annuli and the simulated locations yield simulated values of ρ and γ . The simulated dataset is fit with the assumed model, re-optimizing its parameters and obtaining the best-fit value of the likelihood. This process is repeated to generate 1000 simulated datasets and likelihood values. If the actual best-fit likelihood value is much different from the simulated best-fit likelihoods, the model is probably a poor explanation of the data. The simulation results are shown in Table 4—all of the actual best-fit likelihoods are reasonable according to the simulations except for the likelihood of the minimal model. Even Model 1 passes this goodness-of-fit test despite the strong rejection of the model by the Bayesian model comparisons.

Recommendations. Models 2 and 33 both make excellent fits to the data (Tables 2 and 4) and the two model histograms are extremely similar (Fig. 5 and 7). While there is evidence that Model 33 is better, for most applications we recommend Model 2 because of its simplicity. For critical analysis, Model 33 might be selected. The models are specified by eqs. 4 to 10. The best-fit parameter values are

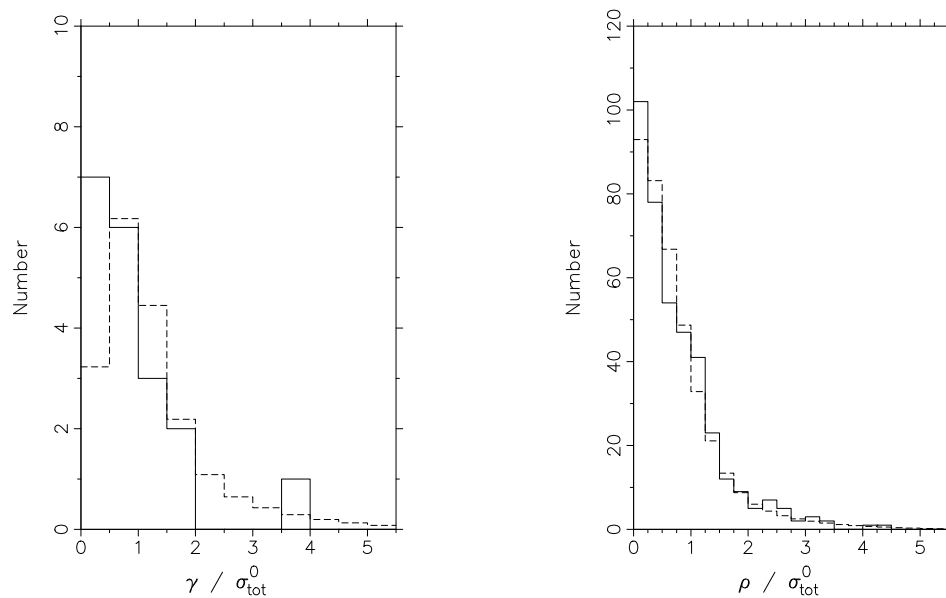


FIG. 7.— Histograms of the data (solid) and Model 33 (dashed). While quantitative measures show Model 33 to be better than Model 2, the model histograms are almost identical.

TABLE 4
GOODNESS-OF-FIT TESTS VIA SIMULATIONS

Model	Best Fit $\log_{10} L_{\text{fit}}$	Mean of Simulations $\log_{10} L_{\text{simu}}$	Standard Deviation of $\log_{10} L_{\text{simu}}$	Fraction of Simulations with $L_{\text{simu}} < L_{\text{fit}}$
0	161.5	293.8	6.5	0/1000
1	211.5	214.9	6.3	0.29
2	220.8	221.6	9.0	0.46
4	212.6	213.4	6.2	0.45
10	223.7	222.2	8.5	0.58
12	222.9	221.0	8.2	0.60
33	223.6	222.8	8.8	0.54

listed in Table 3. If only confidence radii are needed, these may be read from Fig. 8. Because the models are empirically determined using 411 reference locations, confidence radii much beyond 99% have the character of an extrapolation and should be used with caution.

3.2. Comparisons with Previous Analyses

In a preliminary version of this project (Briggs et al. 1998), similar results were obtained. The largest difference is that Model 10 was not presented in that work because it was inferior to Model 12 and Model 33 was not presented because it had not yet been tried. Model 10 has two values of σ_{sys} depending on datatype (6 parameters total), while Model 12 has two values of σ_{sys} for CONT-based locations, but only one value for non-CONT locations (4 parameters total). Model 33 has two values for the core systematic error, but a single value for the fraction and a single-value for the tail systematic error. The current analysis (Table 2) shows Model 33 to be better than Model 12 by a small odds ratio of 8. At this level additional data or different priors might cause the model identified as best to change—this also applies to closely related models not presented. This is not a problem because these three models are based upon the same fundamental ideas (core-plus-tail distribution and datatype dependence) and make nearly identical predictions for location errors.

Reasons to prefer Model 10 are that it seems very plausible that the error distribution of both CONT and non-CONT locations should be best-fit with a core-plus-tail model and there is no reason that the fractions and tail systematic errors must be identical. (This assertion of reasonableness might be termed a “prior”, but we chose not to quantify our inclination.) However, we have recommended Model 33 because it has the best odds ratio and is simpler than Models 10 and 12; in any case these three models provide very similar predictions.

The parameter values of the models are also slightly changed from the preliminary analysis. The differences between the analyses are due to improvements in the IPN locations between the preliminary data releases and the published values, improvements in the BATSE locations between the 4B and 4Br catalog (Paciesas et al. 1998) (also see §3.3) and better rejection of long IPN error boxes. The removal of a small number of outliers due to mistakes had a disproportionate effect on the error analysis.

An earlier work (Graziani and Lamb 1996), which introduced the analysis method used herein, reached

substantially different conclusions. Their best models were intensity dependent, with σ_{sys} a power-law function of σ_{stat} (Model 4) or of the fluence of the burst (Model 8). Table 2 shows Model 2 to be superior to Model 4 by an odds ratio of 3×10^7 and the histograms comparing the observations and Model 4 (Fig. 9) show the fit to be poor. The fluence-based model cannot be analyzed for the full 4Br catalog because fluence values are unavailable for some bursts due to telemetry gaps that are uncorrelated with burst properties. Of the 411 bursts of our comparison sample, 324 have fluence measurements. Table 5 lists model comparisons using these 324 GRBs. Model 2 is superior to Model 8 by an odds ratio of 1×10^8 . The parameter values found for Model 8 are $A = 2.66^\circ \pm 0.12^\circ$ and $\alpha = -0.084 \pm 0.036$. Like Graziani and Lamb (1996), we find the intensity-dependent models to be favored over Model 1 (Tables 2 and 5).

Graziani and Lamb (1996) analyzed the 3B catalog (Meegan et al. 1996) (the 4Br catalog did not yet exist) and restricted the analysis to events with single annuli. They neglected all of the events with γ measurements in order to avoid any locations that might have been used to optimize the location program LOCBURST. Twelve GRBs with γ -values were used to identify which proposed algorithmic improvements were worth implementing (Pendleton et al. 1998). All location algorithm parameter values were determined from laboratory measurements, in-orbit observations of the Crab Nebula and pulsar and from Monte Carlo simulations—none were optimized using GRB measurements. We know of no reason to exclude all γ measurements and judge that there is little ‘circularity’ in using the γ measurements of the twelve ‘study’ bursts. In any case, excluding the data for these twelve events has negligible effects on the results.

The reasons that are probably most important in explaining the difference between our results and those of Graziani and Lamb (1996) are the models tested and revisions to the preliminary IPN data (Hurley et al. 1998a). Using the original 3B BATSE data and the data selections of Graziani and Lamb (i.e., excluding bursts with γ measurements), but using the finalized IPN data, Model 2 is favored over Model 4 by an odds ratio of 400. Adding the γ measurements for all except the twelve ‘study’ bursts, the odds ratio becomes 4700. Unlike Graziani and Lamb, we conclude that there is no evidence for a direct dependence of BATSE systematic location errors on burst intensity.

Because the IPN Supplement emphasizes rela-

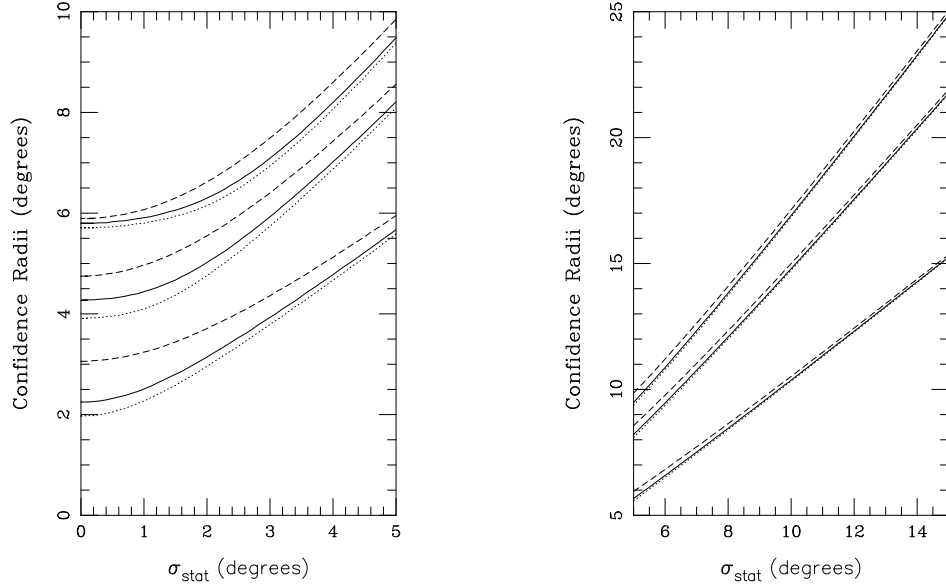


FIG. 8.— Confidence Radii for GRB location as a function of σ_{stat} listed in the 4Br catalog. The curves are based upon Models 2 and 33, as specified in Table 3. The solid curves show the confidence radii for Model 2, the dotted curves the confidence radii according to Model 33 for locations obtained using the CONT datatype, and the dashed curves the radii according to Model 33 for locations obtained using datatypes other than CONT. The bottom trio of curves shows the radii in which the location will fall 68% of the time according to the models, the middle trio the 90% confidence radii, and the top trio the 95% confidence radii.

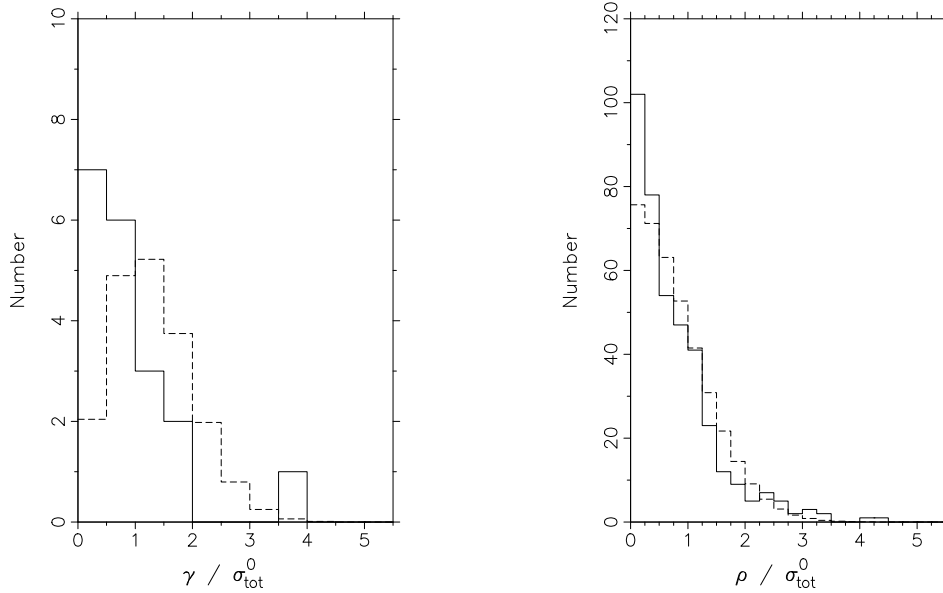


FIG. 9.— Histograms of the data (solid) and Model 4 (dashed). Model 4 predicts too few events at both small ($\rho/\sigma_{\text{tot}}^0 \lesssim 0.25$) and large ($\rho/\sigma_{\text{tot}}^0 \gtrsim 3$) separations.

TABLE 5
 MODELS COMPARISON RESULTS FOR 4BR EVENTS WITH FLUENCE DATA

Model	Description	Number of Parameters	\log_{10} likelihood	\log_{10} Odds Factor
0	Minimal: Systematic Error Assumed to be 1.6°	0	134.0	134.0
1	Single Systematic Error applied to all locations	1	168.2	166.9
2	Core-plus-Tail Systematic Errors	3	177.8	175.0
4	Systematic Error a power law function of statistical uncertainty: $\sigma_{\text{sys}} = A(\sigma_{\text{stat}}/1^\circ)^\alpha$	2	170.4	168.1
8	Systematic Error a power law function of fluence: $\sigma_{\text{sys}} = A(\sigma_{\text{stat}}/1 \times 10^{-5})^\alpha$	2	169.4	166.8

tively bright BATSE bursts (Fig. 2), it is difficult to use IPN data to test the locations of faint bursts. Graziani and Lamb (1996) used extrapolations of Models 4 and 8 to argue that faint BATSE bursts have large systematic errors, e.g., $\sigma_{\text{sys}} = 8^\circ$ for bursts with $\sigma_{\text{stat}} = 10^\circ$, and that the 3B catalog had larger systematic errors for faint bursts than the 1B catalog. Because our analysis finds no evidence that σ_{sys} directly depends on burst intensity, we consider such extrapolations unjustified.

A more direct test of the location accuracy of weak bursts can be made using fluctuations from Cygnus X-1 which triggered BATSE. These fluctuations are almost always near the trigger threshold. The spectra of these fluctuations are similar to GRBs in the energy range (50–300 keV) used for determining locations, but softer at higher energies. Because of the reduced flux above the energy range used for burst locations, the scattering model is less important for locating Cygnus X-1 than for GRBs; however, any intensity dependence of scattering other than the obvious proportionality is implausible. Thirty-nine such events had an average statistical uncertainty σ_{stat} of 12° , but an average separation from the true location of only 10° , implying a 95% confidence upper-limit on σ_{sys} of 7° (Meegan et al. 1996).

There is, however, the possibility of a weak *indirect* correlation of σ_{sys} with burst intensity. The fraction of events located using CONT data decreases with decreasing burst intensity (Fig. 10). The reasons for this trend are correlations between the optimum BATSE datatype for a location, GRB duration, and σ_{stat} : short events are best located with datatypes other than CONT to avoid adding background intervals to the burst data; additionally short events typically have low fluences and thus larger values of σ_{stat} . In Model 33 the only difference between locations obtained using CONT data and other locations is the value of the core systematic error. Coupled with the correlation between datatype and intensity, this datatype dependence of Model 33 implies that a larger fraction of weak bursts have a core systematic error of 2.74° instead of 1.67° . This difference is unimportant for bursts with large values of σ_{stat} . The systematic error is not a direct function of the statistical uncertainty and therefore does not extrapolate to large values for faint bursts.

It seems plausible that the improvement of the models with direct intensity dependencies (Models 4 and 8) over single-parameter models (0 or 1) is due to two correlations: the correlation between intensity and datatype used for the location and the probable

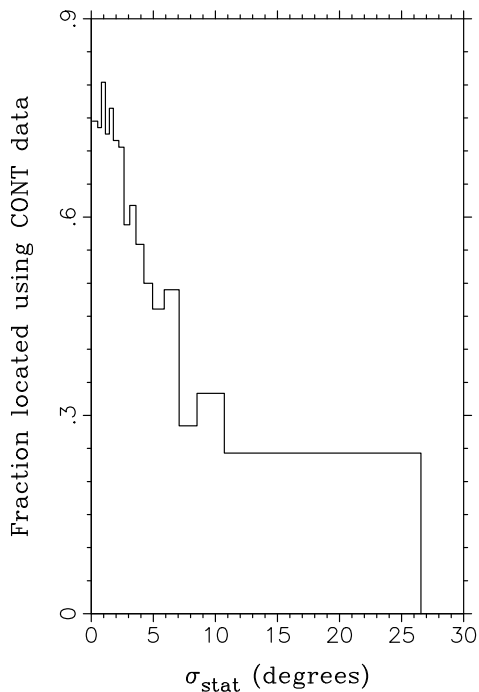


FIG. 10.— Fraction of events located using the CONT datatype versus σ_{stat} . Each of the first 15 bins has 102 locations, while the last bin has 107.

correlation between datatype and systematic error. However, this may not be the case since a model in which σ_{sys} has no dependence on any burst property (Model 2) is favored over Model 4 by a large odds ratio.

3.3. Previous BATSE Catalogs

The locations of the previous BATSE catalogs, 1B (Fishman et al. 1994), 2B (Meegan et al. 1994), 3B (Meegan et al. 1995), and 4B (Paciesas et al. 1997) are superseded by the revised locations of the 4Br catalog (Paciesas et al. 1998), with the exception that bursts of the 3B catalog which are not listed in the 4Br catalog paper have unaltered locations which are considered to be 4Br locations. Key events affecting the quality of the locations were the deterioration of the data availability starting at the end of the 1B catalog due to the failure of the tape recorders on-board CGRO, a substantial recovery of data availability at the end of the 2B catalog due to flight software improvements, and a major improvement in the location algorithm effective with the publication of the 3B catalog (at which time all locations were revised). A lesser algorithmic improvement is implemented with the publication of the 4Br catalog (Paciesas et al. 1998), in which 208 locations are changed from the original 4B catalog.

Table 6 presents analyses of these catalogs for his-

torical interest and to aid in assessing work based upon these catalogs. Since the purpose is to understand BATSE location errors, in all cases the current IPN Supplement data are used rather than the preliminary IPN data available at the time of the publication of a particular BATSE catalog. Only Models 1 and 2 are shown because most of the catalogs are too small to support reliable analysis of models with more than about 3 parameters. The odds ratios favor Model 2 over Model 1 by factors ranging from 4 to 3×10^{13} . The major algorithmic upgrade of LOCBURST can be seen in the comparison of the parameter values for the original 2B and 3B catalogs, or between the original 2B catalog and the equivalent subset of the 4Br catalog. The minor algorithmic improvement between the 4B and 4Br catalogs is not apparent in Table 6, which is not surprising since only 13% of the locations were altered, mostly modestly. A more direct comparison validates the algorithmic upgrade used for the 4Br catalog (Paciesas et al. 1998). There is no evidence in the parameter values for subsets of the 4Br catalog for any time dependence of location quality, especially considering that the parameter values of Model 2 are correlated. In particular, the locations obtained during the period of lesser-quality data (2B–1B) have error model parameters consistent with the other time periods.

4. CONCLUSIONS

TABLE 6
ERROR MODELS FOR VARIOUS DATASETS

Catalog	Trigger Range	Num. of BATSE GRBs	Num. w. IPN data	Num. with γ	Model 1 σ_{sys} (deg)	σ_{sys}^1 (deg)	Model 2 f_1	σ_{sys}^2 (deg)	
Superseded catalogs analyzed using originally published data:									
1B	105	1466	260	54	6	3.4 ± 0.4	1.6 ± 0.4	$0.57^{+0.15}_{-0.19}$	$5.0^{+1.3}_{-0.9}$
2B	105	2230	585	128	18	4.5 ± 0.3	1.8 ± 0.3	0.75 ± 0.07	$9.3^{+1.7}_{-1.4}$
3B	105	3174	1122	264	19	2.88 ± 0.15	1.69 ± 0.22	0.71 ± 0.11	4.9 ± 0.8
4B	105	5586	1637	411	19	2.90 ± 0.12	1.84 ± 0.18	0.74 ± 0.09	5.0 ± 0.7
Subsets of the 4Br catalog:									
full	105	5586	1637	411	19	2.80 ± 0.12	1.85 ± 0.16	0.78 ± 0.08	$5.1^{+0.8}_{-0.6}$
1B	105	1466	263	54	6	2.56 ± 0.30	1.6 ± 0.3	$0.79^{+0.10}_{-0.20}$	$5.4^{+2.5}_{-1.5}$
2B	105	2230	586	128	18	2.80 ± 0.20	1.55 ± 0.26	$0.72^{+0.09}_{-0.13}$	$5.2^{+1.2}_{-0.9}$
2B-1B	1467	2230	323	74	12	3.0 ± 0.3	1.5 ± 0.4	0.67 ± 0.18	$5.1^{+1.5}_{-1.0}$
3B	105	3174	1122	264	19	2.89 ± 0.15	1.77 ± 0.18	0.76 ± 0.09	$5.4^{+0.9}_{-0.7}$
4B-2B	2232	5586	1051	283	1	2.80 ± 0.14	2.08 ± 0.21	$0.84^{+0.07}_{-0.12}$	$5.4^{+1.3}_{-1.0}$
4B-3B	3177	5586	516	147	0	2.61 ± 0.20	2.1 ± 0.4	$0.81^{+0.16}_{-0.35}$	$4.4^{+3.8}_{-1.2}$

This paper presents an improved model of the BATSE GRB location errors. Future work may incorporate improvements such as the incorporation of more locations (BATSE and IPN), additional ‘point’ IPN locations when more interplanetary spacecraft, such as the Near Earth Asteroid Rendezvous (NEAR) mission, are added to the network, the use of locations obtained with BeppoSAX (which was launched several months before the end of the 4Br catalog) and HETE II, and the extension of the analysis to use comparison locations with errors not negligible compared to BATSE (e.g., COMPTEL and WATCH locations). Another possible extension would be to use elliptical error boxes rather than the azimuthally symmetric distributions assumed here. We continue to search for correlations between location errors and other properties. Such correlations might explain why some bursts are in the tail of the location distribution. If we identify a correlation, we might be able to use that knowledge to improve the location algorithm.

The parameter values of model fits to catalogs preceding the 4Br catalog confirm that the location algorithm introduced with the 3B catalog was a significant improvement over the previous algorithm.

The models of this paper are highly significant

improvements over previous models of the BATSE GRB location error distribution. We recommend the three-parameter ‘core-plus-tail’ model (Model 2) for most analyses. There is evidence that a ‘core-plus-tail’ model with core systematic error depending on datatype (Model 33) is superior, and this model can be used for the most critical applications.

A promising use of BATSE and IPN locations is rapid (minutes to hours) optical observations of GRB locations obtained with the BATSE Rapid Burst Response (RBR) System (Kippen et al. 1998), followed by detailed analysis of the smaller error box obtained either with the intersection of a single IPN annulus with the BATSE box or the very small error box obtained by the intersection of a pair of IPN annuli. The RBR locations are obtained by human operators using the standard LOCBURST algorithm and have accuracies consistent with the accuracies of BATSE catalog locations.

MSB, GNP, RMK, and JJB acknowledge NASA Grant NCC8-65 for support. KH is grateful to JPL Contract 958056 for support of Ulysses operations and to NASA Grant NAG5-1560 for support of the IPN. We appreciate the suggestions of the anonymous referee.

APPENDIX

DERIVATION OF $P(\rho)$

The goal is to test the probability density function $p(\gamma)$ for the separation γ between the BATSE location and the true location. In most cases only single IPN annuli are available and therefore only the smallest distances ρ between the BATSE location and the IPN annuli can be determined. In such cases the testing of $p(\gamma)$ must be done indirectly by comparing $p(\rho)$ to the observations. The subject of this Appendix is deriving $p(\rho)$ given $p(\gamma)$, assumed to be the Fisher distribution (eq. 5).

Figure 11 depicts the geometry of comparing a BATSE location to a single IPN annulus. All circles and positions are on the surface of the unit sphere. The IPN annulus, which may not be a great circle, has radius r and is assumed to have a negligible width δr . The coordinate system is chosen so that the center of the IPN annulus is at \hat{z} and the true location \hat{T} is in the xz plane. The BATSE location \hat{B} is at an arbitrary position on the unit sphere.

Locations may be expressed in spherical coordinates (θ, ϕ) , where θ is the angle from \hat{z} and ϕ is the azimuthal angle from \hat{x} (see Fig. 11). Since

$$\rho = |\theta - r|, \quad (\text{A1})$$

the probability density function $p(\rho)$ can be readily obtained from $p(\theta)$. The assumed probability density function is a function of γ , so it is necessary to derive the relationship between the coordinate system (θ, ϕ) and the system (γ, ψ) , where γ is the angle from \hat{T} to \hat{B} and ψ is an azimuthal angle about \hat{T} .

$$\hat{T} = \sin r \hat{x} + \cos r \hat{z}, \quad (\text{A2})$$

$$\hat{B} = \sin \theta \cos \phi \hat{x} + \sin \theta \sin \phi \hat{y} + \cos \theta \hat{z}. \quad (\text{A3})$$

Therefore,

$$\cos \gamma = \hat{T} \cdot \hat{B} \quad (\text{A4})$$

$$= \cos(\theta - r) - \sin \theta \sin r (1 - \cos \phi). \quad (\text{A5})$$

Since the transformation is a rotation, the Jacobean determinant is unity and the transformation between probability density functions is simply $p(\theta, \phi) = p(\gamma, \psi)$. The probability density function is assumed to be rotationally symmetric, so $p(\gamma, \psi) \equiv p(\gamma)$.

Substituting for $\cos \gamma$ from eq. A5 into eq. 5 for the Fisher distribution,

$$p(\theta, \phi) d\Omega = \frac{\kappa}{2\pi(e^\kappa - e^{-\kappa})} e^{\kappa \cos(\theta-r)} e^{-\kappa \sin \theta \sin r (1 - \cos \phi)} d\Omega \quad (\text{A6})$$

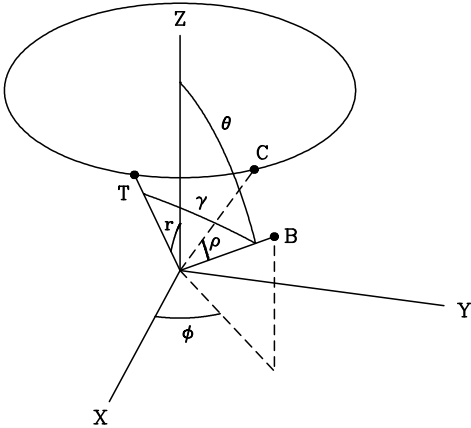


FIG. A11.— Diagram of the geometry relating the true location \hat{T} to the BATSE location \hat{B} . The coordinate system is chosen so that the center of the IPN annulus is at \hat{z} and the true location \hat{T} is in the xz -plane. The annulus has radius r . The BATSE location \hat{B} is at spherical coordinates θ, ϕ . The angle between the true location \hat{T} and the BATSE location \hat{B} is γ , while the angle between the BATSE location \hat{B} and the closest location on the annulus \hat{C} is ρ .

and

$$p(\theta) d\theta = \int_0^{2\pi} d\phi p(\theta, \phi) d\theta \quad (\text{A7})$$

$$= \frac{\kappa}{\pi(e^\kappa - e^{-\kappa})} e^{\kappa \cos(\theta-r)} \int_0^\pi d\phi e^{-\kappa \sin\theta \sin r(1-\cos\phi)} d\theta. \quad (\text{A8})$$

Finally, using formula 8.431.3 of Gradshteyn and Ryzhik (1980),

$$p(\theta) d\theta = \frac{\kappa}{e^\kappa - e^{-\kappa}} e^{\kappa \cos(\theta-r)} \frac{I_0(\kappa \sin\theta \sin r)}{e^{\kappa \sin\theta \sin r}} d\theta. \quad (\text{A9})$$

Including the factor $e^{\kappa \sin\theta \sin r}$ in the last term makes that term more amenable to numerical evaluation (e.g., routine BESSIO of Press et al. (1992) is easily modified in this manner).

Usually there are two values of θ for a value of ρ , corresponding to locations inside and outside of the annulus, so that

$$p(\rho) d\rho = p(\theta = r - \rho) d\theta + p(\theta = r + \rho) d\theta. \quad (\text{A10})$$

In the unusual case that $\rho > r$, only the $\theta = r + \rho$ term contributes.

REFERENCES

- Briggs, M. S., Pendleton, G. N., Brainerd, J. J., Connaughton, V., Kippen, R. M., Meegan, C. & Hurley, K. C. 1998, in AIP Conf. Proc. 428: Gamma-Ray Bursts, ed. C. Meegan, R. Preece & T. Koshut, (New York: AIP), 104
- Fisher, N. I., Lewis, T. & Embleton, B. J. J. 1987, Statistical Analysis of Spherical Data, (Cambridge, England: Cambridge Univ. Press)
- Fishman, G. J., Meegan, C. A., Wilson, R. B., Brock, M. N., Horack, J. M., Kouveliotou, C., Howard, S., Paciasas, W. S., Briggs, M. S., Pendleton, G. N., Koshut, T. M., Mallozzi, R. S., Stollberg, M. & Lestrade, J. P. 1994, ApJS, 92, 229
- Gehrels, N., Chipman, E. & Kniffen, D. A. 1993, in AIP Conf. Proc. 280: Compton Gamma-Ray Observatory, ed. M. Friedlander, N. Gehrels & D. J. Macomb (New York: AIP), 3
- Gradshteyn, I. S. & Ryzhik, I. M. 1980, Table of Integrals, Series, and Products, rev. by A. Jeffrey, Yu. V. Geronimus & M. Yu. Tseytlin, (New York: Academic Press)
- Graziani, C. & Lamb, D. Q. 1996, in AIP Conf. Proc. 384, ed. C. Kouveliotou, M. S. Briggs & G. J. Fishman, (New York: AIP), 382
- Hurley, K. C., Briggs, M. S., Kippen, R. M., Kouveliotou, C., Meegan, C., Fishman, G., Cline, T. & Boer, M. 1998a, ApJS, in press
- Hurley, K. C., Briggs, M. S., Kippen, R. M., Kouveliotou, C., Meegan, C., Fishman, G., Cline, T. & Boer, M. 1998b, ApJS, in press
- Hurley, K. C. 1998, "Interplanetary Network Data", <http://ssl.berkeley.edu/ipn3>
- Kippen, R. M., Connaughton, V., Pendleton, G. N., Barthelmy, S. D., Woods, P., Briggs, M. S., Fishman, G. J., Kouveliotou, C., Robinson, C. R. & Meegan, C. A. 1998, in AIP Conf. Proc. 428: Gamma-Ray Bursts, ed. C. Meegan, R. Preece & T. Koshut, (New York: AIP), 119
- Laros, J. G., Boynton, W. V., Hurley, K. C., Kouveliotou, C., McCollough, M. L., Fishman, G. J., Meegan, C. A., Palmer, D. M., Cline, T. L., Starr, R. D., Trombka, J. I., Boer, M., Niel, M. & Metzger, A. E. 1997, ApJS, 110, 157.
- Laros, J. G., Hurley, K. C., Fenimore, E. E., Klebesadel, R. W., Briggs, M. S., Kouveliotou, C., Meegan, C. A., Cline, T. L., Boer, M. & Niel, M. 1998, ApJS, in press.
- Loredo, T. J. 1990, in Maximum Entropy and Bayesian Methods, ed. P. F. Fougère, (Dordrecht: Kluwer), 81
- Meegan, C. A., Fishman, G. J., Horack, J. M., Brock, M. N., Cole, S., Paciasas, W. S., Briggs, M. S., Pendleton, G. N., Preece, R., Koshut, T. M., Mallozzi, R. S., Kouveliotou, C. & McCollough 1994, published electronically: coss.gsf.nasa.gov/coss
- Meegan, C. A., Pendleton, G. N., Briggs, M. S., Kouveliotou, C., Koshut, T. M., Lestrade, J. P., Paciasas, W. S., Henze, W., McCollough, M. L., Brainerd, J. J., Horack, J. M., Hakkila, J., Henze, W., Preece, R. D., Mallozzi, R. S. & Fishman, G. J. 1996, ApJS, 106, 65
- Paciasas, W. S., Meegan, C. A., Pendleton, G. N., Briggs, M. S., Kouveliotou, C., Koshut, T. M., Lestrade, J. P., McCollough, M., Brainerd, J. J., Hakkila, J., Henze, W., Preece, R. D., Mallozzi, R. S. & Fishman, G. J., 1997, released at coss.gsf.nasa.gov/coss/BATSE.html and on CDROM
- Paciasas, W. S., Meegan, C. A., Pendleton, G. N., Briggs, M. S., Kouveliotou, C., Koshut, T. M., Lestrade, J. P., McCollough, M., Brainerd, J. J., Hakkila, J., Henze, W., Preece, R. D., Mallozzi, R. S. & Fishman, G. J., 1998, ApJS, in press
- Pendleton, G. N., Paciasas, W. S., Mallozzi, R. S., Koshut, T. M., Fishman, G. J., Meegan, C. A., Wilson, R. B., Horack, J. M. & Lestrade, J. P. 1995, Nuc. Instru. & Methods in Phys. Res. A, 364, 567
- Pendleton, G. N., Briggs, M. S., Kippen, R. M., Paciasas, W. S., Stollberg, M., Woods, P., Meegan, C. A., Fishman, G. J., McCollough, M. L. & Connaughton 1998, ApJ, in press
- Press, W. H., Teukolsky, S. A., Vetterling, W. T. & Flannery, B. P. 1992, Numerical Recipes (Cambridge, England: Cambridge Univ. Press)
- Sivia, D. S. 1996, Data Analysis: A Bayesian Tutorial, (Oxford, England: Oxford Univ. Press)